www.czasopisma.pan.pl PAN www.journals.pan.pl
POLSKA AKADEMIA NAUK

Metrol. Meas. Syst., Vol. 24 (2017), No. 2, pp. 381–390.

PAN POLSKA AKADEMIA NAUK

METROLOGY AND MEASUREMENT SYSTEMS

Index 330930, ISSN 0860-8229

www.metrology.pg.gda.pl

M&MS

MEASUREMENT OF SURFACE PROFILE AND SURFACE ROUGHNESS OF FIBRE-OPTIC INTERCONNECT BY FAST FOURIER TRANSFORM

Chern S. Lin[1)], Shih W. Yang[2)], Hung L. Lin[1)], Jhih W. Li[1)]

1) Feng Chia University, Department of Automatic Control Engineering, 100 Wenhwa Road, Seatwen, Taichung, Taiwan (✉ lincs@fcu.edu.tw, +886 4 2451 7250 3900, pon92053@gmail.com, asd940029@gmail.com)

2) National Chiao Tung University, College of Electrical and Computer Engineering, 1001 University Road, Hsinchu, Taiwan (swyang.nctu@msa.hinet.net)

Abstract

This study proposes a surface profile and roughness measurement system for a fibre-optic interconnect based on optical interferometry. On the principle of Fizeau interferometer, an interference fringe is formed on the fibre end-face of the fibre-optic interconnect, and the fringe pattern is analysed using the Fast Fourier transform method to reconstruct the surface profile. However, as the obtained surface profile contains some amount of tilt, a rule for estimating this tilt value is developed in this paper. The actual fibre end-face surface profile is obtained by subtracting the estimated tilt amount from the surface profile, as calculated by the Fast Fourier transform method, and the corresponding surface roughness can be determined. The proposed system is characterized by non-contact measurement, and the sample is not coated with a reflector during measurement. According to the experimental results, the difference between the roughness measurement result of an *Atomic Force Microscope* (AFM) and the measurement result of this system is less than 3 nm.

Keywords: surface profile, surface roughness, fibre end-face, Fast Fourier transform.

1. Introduction

Fibre-optic communication has become the main media of the present communication transmission. For example, the fibre-optic interconnect technology "Thunderbolt" released by Intel transmits data as light signals via optical fibre instead of copper wire [1–2], so the optical fibre and traditional USB joint are interconnected to increase the transmission rate. The Thunderbolt technology has a key fibre-optic interconnect. The entire fibre module comprises three connectors: an optical/electric conversion part (O/E part), a receptacle lens (Re-Lens), and a plug lens. The O/E Part is a connector for the O/E module and optical fibre, laser cut optical fibres are directly inserted in four holes in the front end of the O/E Part, and the end faces of these fibres and the holes are aligned with a co-plane (fibre tips were not polished), as shown in Fig. 1.

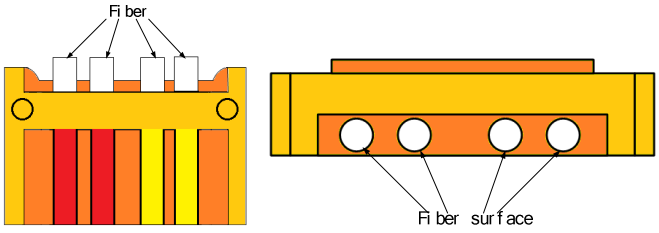

Fig. 1. The O/E Part and a fibre end-face measured in this study.

Article history: received on Aug. 03, 2016; accepted on Dec. 16, 2016; available online on Jun. 30, 2017; DOI: 10.1515/mms-2017-0028.

The fibre end-face roughness after laser cutting has a significant influence on the transmission quality of light signals [3–4]. If the fibre end-face roughness is small, the efficiency of fibre optic coupling is higher. Therefore, developing an efficient system for measuring a surface profile and surface roughness of a fibre end-face is an important issue. Using a contact measurement equipment to check the roughness of fibre end-face is a high-precision scheme [5–6], and as the determinant scan requires a long processing time, the contact probe may scratch the fibre end-face.

The non-contact measurement is another feasible method. In measurement of an insertion loss the laser light shoots into the photovoltaic component joint [7], and the loss value of optical power is indirectly measured to evaluate the quality of fibre end-face. However, to further understand the surface profile and roughness of the optical fibre cutting end-face, combining the machine vision technology with optical interferometry is another appropriate option [8–12]. The phase shifting interferometry shall capture and analyse multiple fringe patterns in order to reconstruct a three-dimensional surface profile of the sample [13–15], where the number of computations is large, but the measurement accuracy is quite high. The Fourier Transform method can reconstruct the surface profile of sample by using only one fringe pattern. Tien *et al.* [16–17]. used a Fizeau interferometer and a Twyman-Green interferometer to obtain interference fringes of thin film, and applied the Fourier Transform method to measure the surface profile and residual stress of thin film [15, 17]. This type of measurement algorithm based on analysing one fringe pattern is faster.

To sum up, this study uses the optical interferometry and a novel imaging system to measure the surface profile and surface roughness of a fibre end-face on an O/E Part [18–19]. The camera captures a fringe pattern of the fibre end-face, and the fringe pattern is analysed using the Fourier transform method to reconstruct the surface profile [19]. However, the obtained surface profile has an additional tilt information, therefore this study proposes a method to eliminate the tilt. Finally, the tilt value is subtracted from the surface profile obtained by the Fourier Transform method, to obtain the actual fibre end-face profile, and the corresponding surface roughness is determined. The difference of RMSs between the roughness measurement results of the proposed method and those obtained by an *Atomic Force Microscope* (AFM) is less than 3 nm.

2. Optical interferometry and novel imaging system

Based on the principle of Fizeau interferometer, the interference fringes of a local fibre end-face on an O/E Part can be observed and recorded by a CCD camera. The proposed image processing algorithm for measuring the surface profile and surface roughness of a fibre end-face is described in the following sections.

2.1. Fringe contrast enhancement

Enhancing the contrast of an interference fringe contributes to the accuracy of the obtained phase distribution. The vertical direction of the surface is detected. A hundred images are collected with an adjustable holder used in image acquisition. Therefore, the contrast of the fibre end-face fringe (Fig. 2a) is enhanced according to the concept of Gamma Correction [20]. A relationship between the fringe grey levels before and after the contrast enhancement is:

$$I(x,y) = \alpha\left(\frac{I_o(x,y)^{\gamma}}{255^{(\gamma-1)}}\right) + \beta, \tag{1}$$

Metrol. Meas. Syst., Vol. 24 (2017), No. 2, pp. 381–390.

where: $I_o(x,y)$ is an original fringe grey level; $I(x,y)$ is a fringe grey level after the contrast enhancement; γ is a correction factor and $\gamma > 0$; α and β are user-defined scale parameters.

When $\gamma > 1$, a bright fringe in Fig. 2a becomes dark; when γ<1, a dark fringe in Fig. 2a becomes bright. After testing, in this study a correction factor γ equal to 0.7 was chosen in order to obtain an appropriate contrast in the darker part. The corresponding results are shown in Fig. 2b. In the darker part the contrast of images (b) is better than images (a).

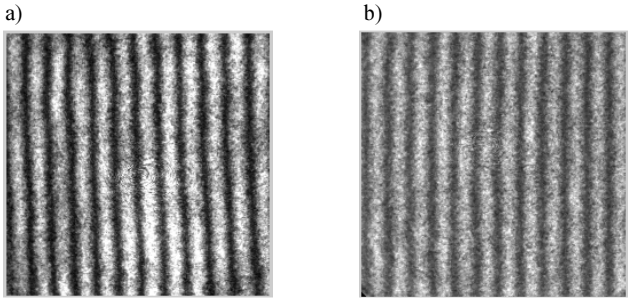

Fig. 2. An original fringe pattern of a local fibre end-face (a); the contrast enhancement result of γ equal to 0.7 (b).

2.2. Phase extraction using Fast Fourier Transform

According to the Fourier Transform method, as proposed by Takeda *et al.* [19], the intensity distribution of a parallel fringe obtained by introducing a spatial carrier can be expressed as:

$$I(x,y) = a(x,y) + b(x,y)\cos[2\pi f_{c,x}x + 2\pi f_{c,y}y + \phi(x,y)], \tag{2}$$

where $a(x,y)$ is a background signal of the fringe pattern; $b(x,y)$ is an amplitude of the interference fringe; $f_{0,x}$ and $f_{0,y}$ are spatial frequencies in x and y directions, respectively and $\phi(x,y)$ is a required phase distribution.

According to the Euler's formula, (2) can be expressed as:

$$I(x,y) = a(x,y) + c(x,y)\exp(j2\pi f_{c,x}x + j2\pi f_{c,y}y) + c^*(x,y)\exp(-j2\pi f_{c,x}x - j2\pi f_{c,y}y), \tag{3}$$

where: $c(x,y) = \frac{1}{2}b(x,y)\exp[j\phi(x,y)]$; $c^*(x,y) = \frac{1}{2}b(x,y)\exp[-j\phi(x,y)]$; and * represents a conjugate complex number.

In order to extract the phase distribution, (3) is processed by Fast Fourier Transform to obtain:

$$I(u,v) = A(u,v) + C(u - f_{c,x}, v - f_{c,y}) + C^*(u + f_{c,x}, v + f_{c,y}), \tag{4}$$

where capital letters represent the results of Fourier Transform; and u and v represent frequencies in x and y directions in the frequency domain, respectively.

As the spatial frequencies of $a(x,y)$ and $b(x,y)$ are lower than $f_{0,x}$ and $f_{0,y}$, there are three major peaks in the spectrum. The peak at the origin of the frequency domain is a background signal $A(u,v)$, while the other two peaks $C(u - f_{c,x}, v - f_{c,y})$ and $C^*(u + f_{c,x}, v + f_{c,y})$, which contain phase distributions, are distributed symmetrically on both sides of the origin, as shown in Fig. 3.

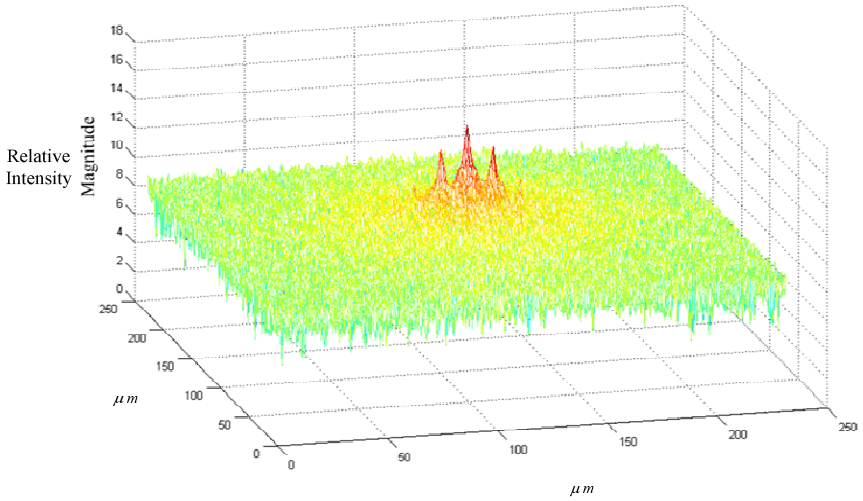

Fig. 3. A spectrum of the fringe pattern after the Fast Fourier Transform.

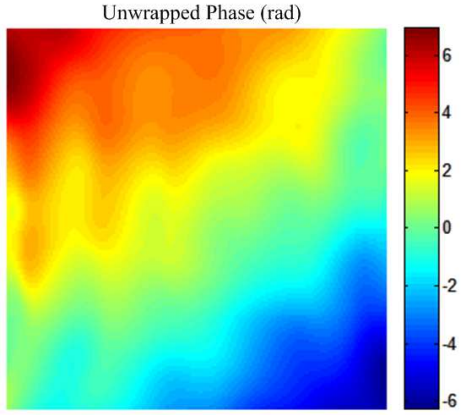

Fig. 4. A continuous phase distribution obtained by the phase unwrapping process.

The spectra $C(u-f_{c,x}, v-f_{c,y})$ or $C^*(u+f_{c,x}, v+f_{c,y})$ can be intercepted correctly by using a bandpass filter. This study filters out $C(u-f_{c,x}, v-f_{c,y})$, and shifts $C(u-f_{c,x}, v-f_{c,y})$ to the origin in order to eliminate the carrier frequency f_c, where $f_c=(f_{c,x}^2+f_{c,y}^2)^{1/2}$. The resulted spectrum is then used in the Inverse Fast Fourier Transform to determine $c(x, y)$. Then, the phase distribution $\phi(x, y)$ can be determined by:

$$\phi(x, y) = \arctan\left(\frac{\mathrm{Im}[c(x, y)]}{\mathrm{Re}[c(x, y)]}\right), \tag{5}$$

where: $\mathrm{Re}[c(x, y)]$ and $\mathrm{Im}[c(x, y)]$ are the actual and imaginary parts of $c(x, y)$, respectively.

The result of (5) is between $-\pi/2$ and $\pi/2$. According to the sign relation between the numerator and denominator of (5), the phase distribution can be corrected to $-\pi$ or π; however, the obtained wrapped phase still has a discontinuity. The phase unwrapping algorithm is introduced in this study to obtain a correct and continuous phase distribution [21], namely,

Metrol. Meas. Syst., Vol. 24 (2017), No. 2, pp. 381–390.

by checking whether the absolute value of the phase difference between each pixel and its adjacent pixel is smaller than π; if the absolute value of the phase difference is larger than π, the phase value of the pixel must increase or decrease the integral multiple of 2π till the absolute value of the phase difference from the adjacent pixel is smaller than π. A continuous phase distribution $\phi'(x, y)$ obtained by the phase unwrapping process is shown in Fig. 4. It is a pseudo colour image mapping results of the entire image.

2.3. Measurement of surface profile and surface roughness

According to the definition of interference equation, the phase difference between a bright fringe and a dark fringe is π, and the corresponding surface height difference is $\lambda/4$, where λ is a wavelength of the light source. Therefore, a surface profile $h(x, y)$ corresponding to the unwrapped phase is:

$$h(x, y) = \frac{\lambda}{4\pi}\phi'(x, y). \tag{6}$$

The result is shown in Fig. 5a. Notice that the surface profile $h(x, y)$ in Fig. 5a contains a tilt value.

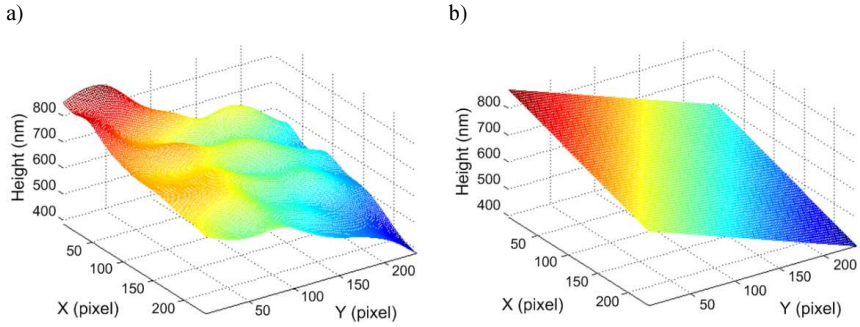

Fig. 5. A surface profile with a tilt value (a); an estimated tilt value (b).

In this study the least square method is used to fit the surface profile obtained by (6) into a plane, where the value of each point in this fitting plane can be approximated as a tilt value corresponding to the surface profile. Let the equation of this fitting plane be:

$$\Delta h(x, y) = Dx + Ey + F, \tag{7}$$

where $\Delta h(x, y)$ is a height of coordinates (x, y) on the fitting plane, *i.e.* the tilt value; D, E and F are parameters of the plane equation.

As the sum of distances from points in $h(x, y)$ to the plane represented by (7) is minimum, the relationship of parameters D, E and F to $h(x, y)$ can be expressed in a matrix form as:

$$\begin{bmatrix} D \\ E \\ F \end{bmatrix} = \begin{bmatrix} \sum_{i=1}^{n} x_i^2 & \sum_{i=1}^{n} x_i y_i & \sum_{i=1}^{n} x_i \\ \sum_{i=1}^{n} x_i y_i & \sum_{i=1}^{n} y_i^2 & \sum_{i=1}^{n} y_i \\ \sum_{i=1}^{n} x_i & \sum_{i=1}^{n} y_i & n \end{bmatrix}^{-1} \begin{bmatrix} \sum_{i=1}^{n} x_i h(x_i, y_i) \\ \sum_{i=1}^{n} y_i h(x_i, y_i) \\ \sum_{i=1}^{n} h(x_i, y_i) \end{bmatrix}, \tag{8}$$

where: n is the total number of pixels in the fringe pattern; (x_i, y_i) are the coordinates of No. i pixel in $h(x, y)$; and $h(x_i, y_i)$ is a height of the pixel (x_i, y_i).

According to the parameters obtained by (8), the tilt value in Fig. 5a can be estimated, as shown in Fig. 5b. The actual fibre end-face surface profile $H(x, y)$ can be calculated by:

$$H(x, y) = h(x, y) - \Delta h(x, y). \tag{9}$$

The surface roughness of the fibre end-face can be calculated based on the result of (9). In this study mean roughness (Ra) and root-mean-square roughness (Rq) are selected as the measurement targets:

$$Ra = \frac{1}{n}\sum_{i=1}^{n} |H(x_i, y_i) - \langle H(x, y)\rangle|, \tag{10}$$

$$Rq = \{\frac{1}{n}\sum_{i=1}^{n} [H(x_i, y_i) - \langle H(x, y)\rangle]^2\}^{1/2}, \tag{11}$$

where $H(x_i, y_i)$ is an actual height of No. i pixel in the fringe pattern; and $\langle H(x, y)\rangle$ is an average of the actual height.

3. Experimental results and discussion

3.1. Experimental setup

This system obtains the fringe pattern of a fibre end-face on the principle of Fizeau interferometer, and analyses the fringe pattern in order to measure the surface roughness. The O/E Part is placed on a mounting device, and an optical flat (λ/20 flat, Edmund Optics) is set up above the O/E Part. A red light semiconductor laser is used as the system light source (λ = 632.8 nm). The laser light is expanded by the fibre bundle, the coaxial light is formed by a beam splitter, and two light beams with similar intensities are split. One light beam irradiates the optical flat (reference surface) through a high magnification objective lens, while the other light beam irradiates the fibre end-face of the O/E Part; this beam is then reflected to the beam splitter to form the interference fringe with the reference light. Finally, a CCD camera captures the fringe pattern. The proposed system framework is shown in Fig. 6.

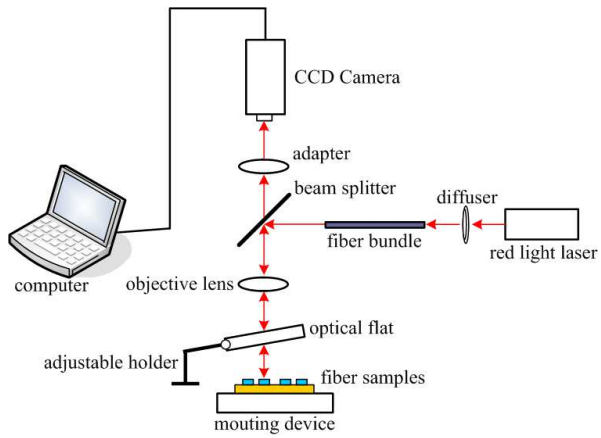

Fig. 6. A structure of the proposed system.

Metrol. Meas. Syst., Vol. 24 (2017), No. 2, pp. 381–390.

The optical fibre on the O/E Part examined in this study consists of a fibre core, cladding, and coating. The refractive index of the cladding is lower than that of the fibre core. The coating has a high toughness, which protects the optical fibre against damage. This optical fibre is a multimode fibre from *Fibre Optic Communications, Inc*. (FOCI), with a diameter of 125 μm; a diameter of the fibre core is 62.5μm, and the red or yellow plastic coating has a diameter of 600 μm (Fig.1).

3.2. Measurement results and analysis

The fringe pattern of the fibre end-face sample examined in this study is shown in Fig. 2a, and represents a region with an actual size of about 40 um × 40 um. The method proposed in Section 2 is used for non-contact measurement of a surface profile and a surface roughness. First, the contrast of the interference fringe is enhanced, and the result is processed by the Fast Fourier Transform in order to obtain a corresponding spectrum. The required side-lobe signal is intercepted by a filter, and processed by the Inverse Fourier Transform to obtain the phase value; a continuous phase distribution can be obtained by using the phase unwrapping algorithm. Finally, the surface profile of the fibre end-face can be obtained by multiplying the unwrapped phase by a constant and deducting the tilt value. The result is shown in Fig. 7.

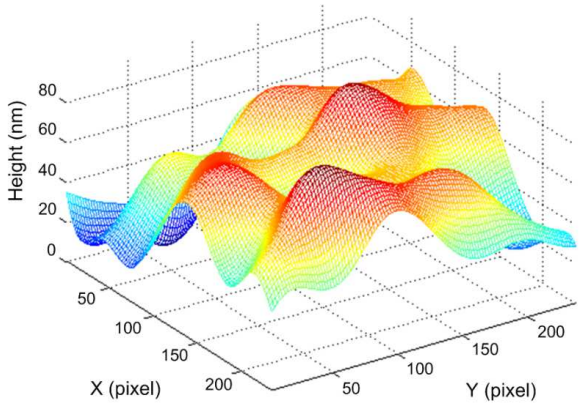

Fig. 7. A local surface profile of the fibre end-face obtained using the proposed method.

In order to validate the accuracy of the proposed method, the same fibre end-face sample was measured by an AFM for comparison. AFM is a contact surface profile measurement equipment, and its measurement accuracy is very high. However, the scanning speed is relatively low, therefore the contact probe may damage the surface structure of sample. In addition, as the scanning area of AFM is limited, and the gap between the fibre core edge and the surface height of the O/E Part is large, the AFM probe is likely to break while scanning the fibre core edge; therefore it is inapplicable to inspection of the production line. In the experiment, AFM measured only the local fibre end-face close to the fibre core centre to calculate its roughness. The area measured by AFM may be not completely consistent with the area measured by the proposed method; however, the surface roughness of the sample in the same process varies only slightly. Therefore, the measurement result of AFM still can be an index in evaluating the accuracy of this method. The measurement result of AFM is shown in Fig. 8. *Rq* corresponding to this local area is equal to 26.1 nm, and *Ra* – to 18.1 nm. *Rq* calculated by the proposed method is equal to 23.4 nm, and *Ra* – to 19.2 nm. Comparison of the measurement results of this method with those of AFM shows that the *Rq* difference is equal

to 2.7 nm, and the *Ra* difference – to 1.1 nm. Thus, the difference is within 3 nm. The scope of random variation in results and differences can be neglected as statistically insignificant.

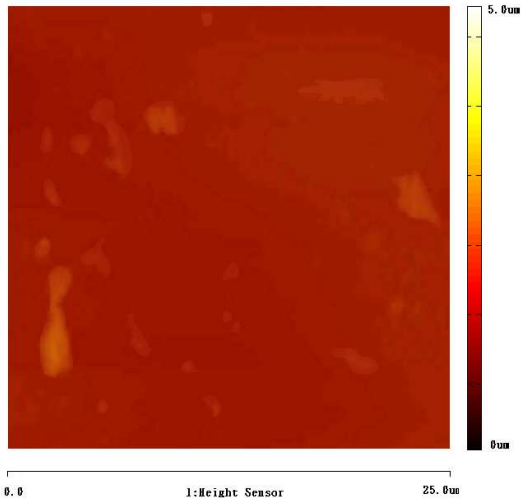

Fig. 8. The measurement result of AFM of the local part of sample.

The measurement result of AFM can validate the accuracy of the method presented in this study. The structure of it is simple, and its cost is lower than AFM's [21]. In addition, when a contact equipment is used to measure the body surface of unknown materials, SEM is sometimes required to evaluate the measurement feasibility in advance. However, this study concerns a non-contact measurement; the surface profile of sample can be reconstructed, and the surface roughness can be measured by only one fringe pattern with a spatial carrier, which is quite easily visualised and convenient. It should be considered in this system that, when a magnitude of the introduced spatial carrier is changed by adjusting the angle of the optical flat if the introduced spatial carrier is too small, the side-lobe peak position and background signal peak position would be too close to each other after applying the Fast Fourier Transform. As a result of this phenomenon, a partial background signal will be captured along with capturing the side-lobe, resulting in a measurement error. If the introduced spatial carrier is too large, the fringe contrast decays and cannot be correctly analysed.

4. Conclusions

As the flatness of a fibre end-face after laser cutting can significantly influence the coupling efficiency of the O/E Part and the fibre optic coupler, in this study there is proposed a surface profile and roughness measurement system as a solution to analysing a fibre end-face. The hardware is based on the Fizeau interferometer in order to obtain the interference fringe of a local fibre end-face on the O/E Part. Then, the phase data are calculated using the Fast Fourier Transform, and the local surface profile and surface roughness are reconstructed. In addition, the accuracy of the proposed algorithm is validated experimentally and with a program. Compared with the measurement result of AFM, the corresponding roughness difference is less than 3 nm. This system can assist manufacturers to accurately screen too rough optical fibre samples, and its measurement results can be a reference frame for improving the process.

Metrol. Meas. Syst., Vol. 24 (2017), No. 2, pp. 381–390.

Acknowledgements

This research project was supported by the Ministry of Science and Technology, under Grant No. MOST 105-2221-E-035 -027.

References

[1] Chow, C.W., Yeh, C.H., Yang, L.G., Sung, J.Y., Huang, S.P. (2012). Design and characterization of large-core optical fiber for Light Peak applications. *Opt. Eng.*, 51(1), 015006.

[2] Yajima, Y., Watanabe, H., Kihara, M., Toyonaga, M. (2011). Optical performance of field assembly connectors using incorrectly cleaved fiber ends. *Opto-Electronics and Communications Conference (OECC)*, 617–618.

[3] Berdinskikh, T., Bragg, J., Tse, E., Daniel, J., Arrowsmith, P., Fisenko, A., Mahmoud, S. (2002). The contamination of fiber optics connectors and their effect on optical performance. *Optical Fiber Communication Conference and Exhibit*, 617–619.

[4] Garnaes, J., Kofod, N., Kühle, A., Nielsen, C., Dirscherl, K., Blunt, L. (2003). Calibration of step heights and roughness measurements with atomic force microscopes. *Precision Engineering*, 27(1), 91–98.

[5] Poon, C.Y., Bhushan, B. (1995). Comparison of surface roughness measurements by stylus profiler. AFM and non-contact optical profiler. *Wear*, 190(1), 76–88.

[6] Kihara, M., Okada, M., Hosoda, M., Iwata, T., Yajima, Y., Toyonaga, M. (2012). Tool for inspecting faults from incorrectly cleaved fiber ends and contaminated optical fiber connector end surfaces. *Optical Fiber Technology*, 18(6) 470–479.

[7] Lin, C.S., Lin, C.H., Lin, C.C., Yeh, M.S. (2010). Three-dimensional profile measurement of small lens using subpixel localization with color grating. *Optik*, 121(23), 2122–2127.

[8] Lin, C.S., Loh, G.H., Tien, C.L., Lin, T.C., Chiou, Y.C. (2013). Automatic Optical Inspection System for the Micro-lens of Optical Connector with Fuzzy Ratio Analysis. *Optik*, 124(17), 3085–3090.

[9] Lu, J., Chen, J., Xie, J., Wang, F., Tan, Z. (2013). A novel automatic method of fringe counter for equally tilting fringe. *Optik*, 124(15), 2062–2066.

[10] Lin, C.S., Tzeng, G.A., Cheng, C.T., Lay, Y.L., Tien, C.L. (2014). An Automatic Optical Inspection System for the Detection of Three Parallel Lines in Solar Panel End Face. *Optik*, 125(2), 688–693.

[11] Yang, S.W., Lin, S.K. (2014). Automatic Optical Inspection System for 3D Surface Profile Measurement of Multi-Microlenses using Optimal Inspection Path. *Measurement Science & Technology*, 25(7), 075006.

[12] Wang, W.H., Wong, Y.S., Hong, G.S. (2006). 3D measurement of crater wear by phase shifting method. *Wear*, 261(2), 164–171.

[13] Fu, Y., Wang, Z., Yang, J., Wang, J., Jiang, G. (2014). Three-dimensional profile measurement of the blade based on multi-value coding. *Optik*, 125(11), 2592–2596.

[14] Chatterjee, S., Kumar, Y.P., Bhaduri, B. (2007). Measurement of surface figure of plane optical surfaces with polarization phase-shifting Fizeau interferometer. *Optics and Laser Technology*, 39(2), 268–274.

[15] Tien, C.L., Yang, H.M., Liu, M.C. (2009). The measurement of surface roughness of optical thin films based on fast Fourier transform. *Thin Solid Films*, 517(17), 5110–5115.

[16] Hu, E., Zhu, Y. (2013). 3D online measurement of spare parts with variable speed by using line-scan non-contact method. *Optik*, 124(13), 1472–1476.

[17] Tien, C.L., Zeng, H.D. (2010). Measuring residual stress of anisotropic thin film by fast Fourier transform. *Optics Express*, 18(16), 16594–16600.

[18] Park, C.W., Ryu, J.Y. (2008). Development of a new automatic gamma control system for mobile LCD applications. *Displays*, 29(4), 393–400.

[19] Takeda, M., Mutoh, K. (1983). Fourier transform profilometry for the automatic measurement of 3-D object shapes. *Applied Optics*, 22(24), 3977–3982.

[20] Zhao, M., Huang, Q.H., Zhu, L.J., Qiu, Z.M. (2015). Automatic laser interferometer and vision measurement system for stripe rod calibration. *Metrol. Meas. Syst.*, 22(4), 491–502.

[21] Macy, W.W. (1983). Two-dimensional fringe-pattern analysis. *Applied Optics*, 22(23), 3898–3901.